

Exchange anisotropy in epitaxial and polycrystalline NiO/NiFe bilayers

R. P. Michel* and A. Chaiken†

Materials Science and Technology Division, Lawrence Livermore National Laboratory, Livermore, California 94551

C. T. Wang

Department of Materials Science and Engineering, Stanford University, Palo Alto, California 94305

L. E. Johnson

Materials Science and Technology Division, Lawrence Livermore National Laboratory, Livermore, California 94551

(Received 16 January 1997; revised manuscript received 3 March 1998)

(001)-oriented NiO/NiFe bilayers were grown on single crystal MgO (001) substrates by ion beam sputtering in order to determine the effect that the crystalline orientation of the NiO antiferromagnetic layer has on the magnetization curve of the NiFe ferromagnetic layer. The simplest model predicts no exchange anisotropy for the (001)-oriented NiO surface, which in its bulk termination is magnetically compensated. Nonetheless exchange anisotropy is present in the epitaxial films, although it is approximately half as large as in polycrystalline films that were grown simultaneously. The surface anisotropy in the epitaxial films is found to contain cubic and unidirectional components, while that in the polycrystalline film is best described by a uniaxial plus unidirectional anisotropy. Experiments indicate that differences in exchange field and coercivity between polycrystalline and epitaxial NiFe/NiO bilayers couples arise due to variations in induced surface anisotropy. Implications of these observations for models of induced exchange anisotropy in NiO/NiFe bilayer couples will be discussed. [S0163-1829(98)07438-4]

I. INTRODUCTION

Exchange anisotropy refers to the effect that an antiferromagnetic (AF) layer grown in contact with a ferromagnetic (FM) layer has on the magnetic response of the FM layer.¹ Exchange anisotropy is one of several magnetic interfacial interactions, which include interlayer coupling in multilayers, that have been intensively studied in recent years. The most notable changes in the FM hysteresis loop due to the surface exchange coupling are a coercivity enhanced over the value typically observed in films grown on a nonmagnetic substrate, and a shift in the hysteresis loop of the ferromagnet away from the zero field axis. The characteristics of the AF layer and the interface between the two layers that produce the strongest exchange bias are not well understood. Experimental studies and theoretical models²⁻⁵ indicate that intrinsic magnetic properties of the AF such as the magnetocrystalline anisotropy, exchange stiffness and crystalline texture,⁶⁻⁹ as well as extrinsic properties such as grain size, domain size and interface roughness^{8,10,11} may influence the resulting response of the FM. Unfortunately, it is difficult to manipulate these properties independently, or to probe the magnetic structure of the bilayer interface directly.

Exchange couples which incorporate FeMn, NiMn, PdMn, IrMn, Pd-Pt-Mn, NiO, and NiCoO antiferromagnetic layers are currently under study for use in magnetoresistive sensors and magnetoresistive and spin-valve-based hard disk readback heads.¹² The exchange anisotropy is employed to achieve the optimum sensitivity in the sensor and to reduce noise by stabilizing domains.¹³⁻¹⁵ In this paper we focus on the oxide AF materials which share the same rocksalt crystal structure. The AF spin configurations and exchange coupling properties of the Mn-based materials are significantly differ-

ent from the oxide materials and thus must be considered separately. The oxide films proposed for applications are polycrystalline with relatively small grain sizes. Achieving a clearer understanding of how magnetocrystalline anisotropy and texture influence the exchange anisotropy, however, requires that films with a high degree of crystalline perfection be examined as well.

Typically NiFe is deposited on top of NiO to form a NiFe/NiO exchange couple. A field of 20–200 Oe is applied during deposition to induce a uniaxial anisotropy in the NiFe layer. The interaction of the aligned NiFe spins at the interface with the NiO during deposition influences the AF spins in the NiO since the applied field is too weak to induce ordering in the NiO spins directly. In turn the NiO spin arrangement stores the exchange bias information and induces a unidirectional surface anisotropy in the NiFe. Heating bilayers above the blocking temperature T_b and cooling in a field has been variously reported to increase¹⁶ and to decrease^{13,17} the interfacial exchange field H_E relative to the as-deposited values. How the magnitude of the deposition field or the cooling field influences H_E has not been well established in the case of oxide antiferromagnets,¹⁸ although a striking change of sign in the exchange bias field has been observed with large deposition fields in the Fe/FeF₂ system.¹⁹

The NiO spin structure is relatively simple, however the large number of domain configurations and domain walls in a multidomain sample make theoretical models of exchange anisotropy in NiO/NiFe bilayers considerably more challenging.²⁰⁻²³ NiO has a cubic FCC NaCl crystal structure above its Néel temperature T_N . Below the Néel temperature there is a slight distortion of the NiO lattice in a $\langle 111 \rangle$ direction ($\Delta l/l \approx 4.5 \times 10^{-3}$).²⁴ A strong negative uniaxial

anisotropy accompanies the contraction, resulting in an easy plane defined by $K_1 \approx 1 \times 10^6$ erg/cm³.²³ Sheets of ferromagnetically aligned spins form in the (111) planes defined by the contraction axis,²¹ with the Ni spins in neighboring sheets oppositely aligned. Within a (111) plane the direction of the spin axis is determined by a second three fold anisotropy (K_3) that is roughly three orders of magnitude weaker than K_1 .^{24,25}

The AF domain configurations in NiO have been studied both experimentally and theoretically. There are four possible (111) directions in a NiO crystal from which the contraction axis may choose, and three spin directions once the contraction axis is defined. Thus there are $4 \times 3 = 12$ distinct possible AF domain configurations in NiO below T_N . Since the four (111) directions in the cubic NiO are nominally equivalent, local inhomogeneities break the symmetry and determine which (111) axis becomes the contraction axis in different regions of the crystal. External applied magnetic fields and strain can make one (111) direction more kinetically favorable, and thereby influence the distribution of AF domains. The magnetic susceptibility of the NiO is largest parallel to the contraction axis (and perpendicular to the planes of spins), so this axis tends to align parallel to strong applied fields.²⁶ Once the sample temperature has been lowered below the Néel temperature, domain walls become strongly pinned^{22,26,27} and extremely large fields are required to change the AF domain configuration.

In this study, we compare the magnetic properties of polycrystalline and epitaxial (001) NiO/NiFe bilayers deposited simultaneously. We also compare epitaxial (001) NiO/NiFe bilayers with the deposition bias field, H_b , aligned along different in-plane NiO crystalline axes. The results of these studies are interpreted in terms of induced anisotropies at the NiO/NiFe interface.

II. EXPERIMENTAL METHODS

The single films and bilayers were grown in a multilayer deposition system using ion beam sputtering (IBS). The system has been described in detail elsewhere.^{28,29} Single crystal polished (001) oriented MgO substrates and Si substrates with native oxide layers were placed side by side in substrate holders with bias magnets. The bias magnets produce a uniform magnetic field, H_b , of 300 Oe at the substrate surface. The substrate temperature was monitored but not controlled and reached about 80 °C during deposition. The NiO layers were grown using a new IBS process.³⁰ The NiO is deposited by directly sputtering a NiO target³¹ with a neutralized 750V, 30 mA Ar-ion beam which produces a deposition rate of about 0.2 Å/sec. No additional reactive gas is introduced during the deposition. The NiFe layers were then grown immediately on top of the NiO using a 500V, 20 mA ion beam without neutralization. The Ar gas pressure during deposition was typically 0.25 mTorr. The Ni:O ratio of films produced using this process was measured using Rutherford back-scattering and was determined to be 1:1 to within 1%. NiFe films were deposited from a Ni₈₁Fe₁₉ sputter target.

The morphology of the NiO/NiFe bilayers was probed using x-ray diffraction (XRD). Symmetric x-ray scans were performed on an 18 kW Rigaku rotating anode diffractometer with a diffracted beam monochromator using Cu K_α

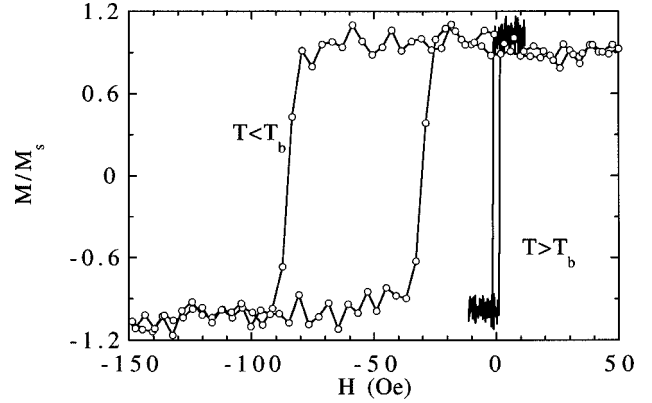


FIG. 1. Hysteresis loops of the same polycrystalline NiO 500 Å/NiFe 100 Å bilayer film are shown, one at a temperature below the blocking temperature, T_b , of NiO and one above T_b . Above T_b , the NiFe behaves as a free layer, magnetically the same as a NiFe layer deposited on a nonmagnetic substrate. Below T_b the interfacial exchange interaction induces a unidirectional anisotropy which shifts the NiFe loop away from the zero field axis and raises its coercivity.

radiation. Phi scans were performed on a four-circle goniometer using Cu radiation at Stanford University.

The magnetic properties of the bilayer films were measured with a vibrating sample magnetometer (VSM) equipped with two sets of orthogonal pick-up coils. The use of two sets of pick-up coils allows the simultaneous measurement of both the longitudinal and transverse magnetization curves, as is often done with Kerr magnetometry.³² Unless otherwise specifically stated, all magnetization data were taken at room temperature. The magnetization curve of a 500 Å thick NiFe film grown on MgO (001) and Si (not shown) shows that H_b applied during deposition induces a uniaxial anisotropy in the NiFe. The value of the uniaxial anisotropy is determined from the hard axis saturation field, H_s , to be $K_u = 2000$ erg/cm³ given that $H_s = 2K_u/M_s$ in the polycrystalline NiFe film. In addition to K_u we also observe a four-fold magnetocrystalline anisotropy in the epitaxial NiFe film of about $K_1 = -500$ erg/cm³ [$H_s = 2(K_u + K_1)/M_s$ for a $\langle 110 \rangle$ hard axis in the (001) plane]. These values are consistent with those expected for NiFe films.³³

III. EXPERIMENTAL RESULTS

Hysteresis loops of a NiO(500 Å)/NiFe(100 Å) bilayer couple measured below and above the NiO blocking temperature, T_b , are shown in Fig. 1 and illustrate the effects of the interface exchange interaction. Above the blocking temperature ($T_b = 200$ °C $<$ $T_N = 240$ °C), the NiO spins are thermally fluctuating and the NiFe film shows evidence only of its usual induced uniaxial anisotropy. The NiFe film has an easy axis coercivity of about $H_{ce} = 2$ Oe, and a hard axis saturation field (not shown) of about $H_s = 5$ Oe. After cooling to room temperature in an external magnetic field, the NiO spins are frozen and the interfacial magnetic interaction induces a unidirectional anisotropy on the NiFe film which shifts the NiFe hysteresis loops away from the zero field axis by an amount H_E . The direction of the shift depends on the orientation of the NiFe layer magnetization during field cooling. In addition to the loop shift, the interfacial interaction

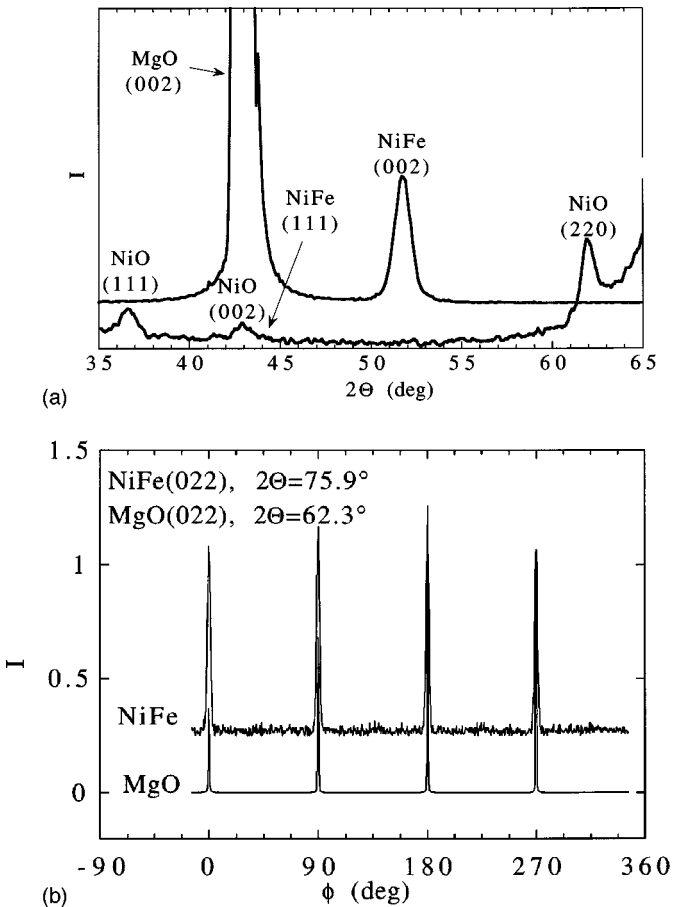


FIG. 2. Comparison of x-ray spectra from NiO 500 Å/NiFe 100 Å bilayer films deposited simultaneously on polished single crystal MgO (001) and oxidized Si substrates. The bottom scan in (a) shows that the NiO on the oxidized silicon substrate is polycrystalline with a grain size of approximately 150 Å. The top scan shows the NiO (111) and (022) Bragg peaks are absent in the bilayer grown on MgO. The MgO (002) substrate peak obscures the presence of the NiO (002) peak. A strong reflection is present from the NiFe (001) planes. In (b), phi scans at the NiFe (022) and the MgO (022) Bragg angles are shown. The NiFe layer is epitaxially oriented relative to the MgO substrate, confirming that the NiO layer is also epitaxial.

increases the coercivity dramatically. Perpendicular to the loop shift direction, the hard axis loop (not shown) passes nearly linearly through zero with almost no coercivity. The $1/t_{\text{NiFe}}$ thickness dependence of H_E and H_{ce} expected from the interfacial origin of these effects, is well established.¹³

A comparison of the XRD spectra for NiO/NiFe bilayers grown simultaneously on MgO (001) and oxidized silicon is shown on Fig. 2. The films deposited on oxidized Si wafers are polycrystalline as shown by the presence of (111), (002), and (022) NiO Bragg peaks. The average grain size calculated using the Scherrer formula from the full width at half maximum (FWHM) of the peaks is 100 Å to 200 Å. Because the NiO and MgO crystal structures are nearly identical with only slightly different lattice parameters, (MgO: $a=4.213$ Å, NiO: $a=4.177$ Å or 0.9% difference) the NiO (002) Bragg peak of the film on MgO is obscured under the strong substrate peak. No NiO (111) or (022) Bragg peak intensity was observed in the XRD spectra of the bilayer grown on

MgO, however. Instead a strong (002) peak from the NiFe deposited on the NiO was present with a correlation length limited by the thickness of the film (100 Å) and a rocking curve width of 1° – 2° FWHM. Phi scans at the NiFe (011) peak position show that the NiFe layer grown on top of the NiO layer is epitaxially oriented relative to the MgO substrate [Fig. 2(b)]. The epitaxy of the NiFe shows that the intermediate NiO layer is also oriented in-plane with respect to the MgO substrate. As discussed in the previous section, NiFe films grown directly on MgO (001) were also found to be epitaxial. Comparison of Kiessig fringes in the low-angle symmetric XRD spectra (not shown) indicate that the interfaces of the epitaxial bilayer are rougher (8–12 Å rms) than the polycrystalline bilayer (2–3 Å rms).

The hysteresis loops of polycrystalline and epitaxial NiO (500 Å)/NiFe (100 Å) bilayers grown simultaneously are shown in Fig. 3. In the epitaxial film the bias field during deposition H_b was applied along an MgO [100] axis. Hysteresis loops parallel and perpendicular to H_b are shown. The polycrystalline bilayer [Fig. 3(a)] illustrates the usual exchange anisotropy behavior: there is a shift in the easy axis hysteresis loop of $H_E=52$ Oe and an increase in the NiFe coercivity from its free value of about $H_{ce}=2$ Oe to $H_{ce}=30$ Oe. The hard axis loop shows almost zero coercivity and saturates at about $2H_E$. The loop parallel to H_b for the epitaxial bilayer [Fig. 3(b)] shows a shift of $H_E=20$ Oe and a coercivity of $H_{ce}=26$ Oe. The shape of the hard axis magnetization (perpendicular to H_b) in the epitaxial film is qualitatively different from the nearly linear hard axis loop observed in the polycrystalline films. Figure 3(c) shows transverse magnetization data for the polycrystalline and epitaxial films with $H \perp H_b$, and indicates the nonlinearity in the epitaxial bilayer's hard axis loop is due to a nearly 90° reorientation of the magnetization vector.

In Fig. 4 another set of magnetization data for polycrystalline and epitaxial NiO/NiFe bilayers grown simultaneously is shown but now with H_b , the bias field applied during deposition, aligned with an in-plane MgO [110] axis. The polycrystalline bilayer [Fig. 4(a)] has an exchange field of $H_E=66$ Oe and an easy-axis coercivity of $H_{ce}=34$ Oe. The hard axis loop once again saturates at about $H_s=2H_E$ and has coercivity less than 1 Oe. The epitaxial bilayer [Fig. 4(b)] has $H_E=36$ Oe, and $H_{ce}=42$ Oe. The hard axis magnetization data shown in Figs. 4(b) and 4(c) shows similar behavior to that seen in Figs. 3(b) and 3(c). The similarity between Figs. 3(b) and 4(b) reveals that the nonlinearity observed in the hard axis magnetization curves of the epitaxial films is induced by H_b and is not referenced to the underlying crystal structure of the NiO. The variation in H_E for the polycrystalline samples shown in Figs. 3(a) and 4(a) results from uncontrolled variations in the deposition conditions and serves as a measure of the run-to-run reproducibility of the growth.

We have grown epitaxial bilayers in reverse order to better understand why this configuration typically shows lower exchange anisotropy than do bilayers with NiO on the bottom.³⁴ Figure 5 shows easy axis magnetization loops for NiFe 100 Å/NiO 500 Å bilayers grown simultaneously on oxidized silicon and MgO (001) substrates. In this configuration the choice of substrate has much less effect on the hysteresis loop. The exchange shift is $H_E=13$ Oe and H_{ce}

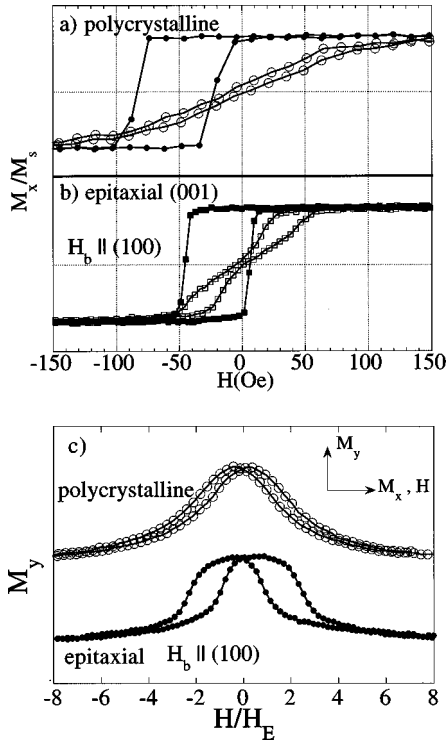


FIG. 3. Magnetization data for two NiO 500 Å/NiFe 100 Å bilayer films deposited simultaneously. In (a) the easy-axis (H parallel to H_b , the bias field during growth) and hard-axis (H perpendicular to H_b) magnetization curves of the polycrystalline bilayer are shown. The easy-axis loop is shifted by $H_E = 52$ Oe due to interfacial exchange anisotropy with the NiO. (b) shows the same measurement as in (a) for an epitaxial (001) bilayer deposited on MgO. The bias field, H_b , applied during deposition was aligned parallel to an in-plane MgO (100) axis. The easy-axis loop is shifted by $H_E = 20$ Oe. Discontinuities in the hard-axis loop reveal the presence of a cubic induced anisotropy term that produces a local energy minimum parallel to the applied field and perpendicular to H_b . In (c) the transverse hard axis magnetization, M_y , for the polycrystalline (open circles) and epitaxial (filled circles) are compared. The smooth curve of the polycrystalline M_y loop shows the magnetization vector rotates continuously as the applied field varies. The plateau in the epitaxial M_y loop confirms that the NiFe moment turns discontinuously from a local energy minimum parallel to the applied field to the deep unidirectional energy minimum perpendicular to it.

$= 5$ Oe in both films. XRD shows that both NiO films are polycrystalline. These data demonstrate that the growth mode of NiO on NiFe is significantly different than that of NiFe on NiO, which explains the difference in the exchange anisotropy observed in the two configurations. Recently, however, large bias fields (0.04 erg/cm²) were reported in “top” spin valves grown with the NiO layer on top of a NiFe layer using reactive RF sputtering.³⁵

IV. ANALYSIS

In order to model the field dependence of the NiFe magnetization, we start by defining the simplest energy equation that contains only a unidirectional anisotropy term and a Zeeman term describing interaction with the external field. We proceed by assuming the magnetization reverses by co-

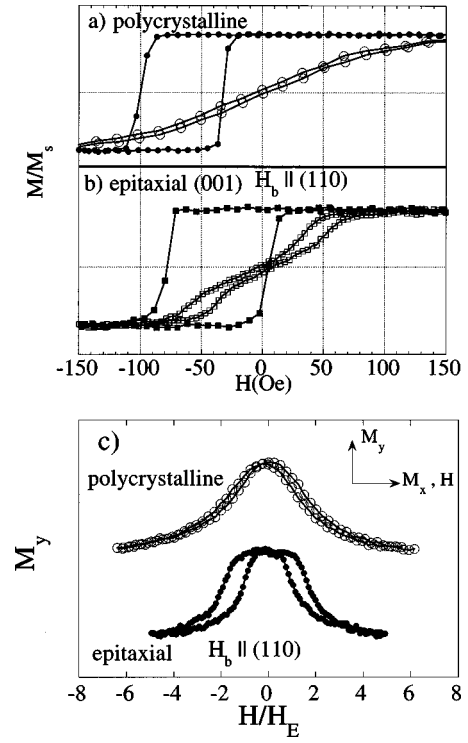


FIG. 4. The same measurements as shown in Fig. 3 for a second set of simultaneously deposited polycrystalline and epitaxial bilayers except that here H_b , the bias field during deposition, was applied parallel to an in-plane MgO (110) axis. For the polycrystalline films in (a) the easy-axis loop is shifted by $H_E = 66$ Oe. In (b) the epitaxial film has $H_E = 36$ Oe. (c) shows the transverse hard axis magnetization loops. The data are qualitatively similar to those in Fig. 3, particularly the observation of discontinuities indicating a cubic anisotropy with minima referenced to the bias field axis. Thus the cubic anisotropy is induced by the bias field and is not influenced by the orientation of H_b relative to the NiO crystal axis.

herent rotation, and that the anisotropy at the interface remains constant during NiFe reversal. Recent results, however, using a magneto-optic indicator film technique³⁶ and Kerr microscopy³⁷ indicate the magnetization in these films reverses by incoherent rotation for fields applied along the

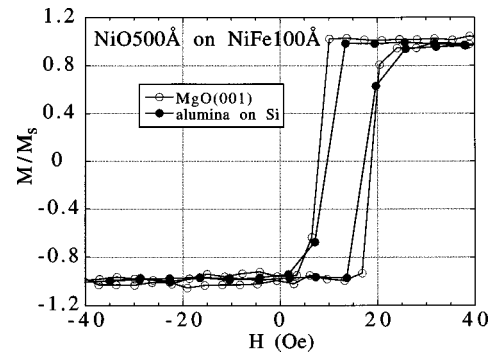


FIG. 5. Easy axis magnetization for two bilayer films deposited in reverse order simultaneously on MgO and an oxidized silicon substrate. Both NiO layers grown on NiFe were polycrystalline. The exchange bias fields and coercivities of the two films are the same. Differences in the growth of NiO on NiFe compared to NiFe on NiO lead to the reduced exchange anisotropy observed in these films.

hard axis and through nucleation and growth of domain walls, for fields applied along the easy axis. The coherent rotation approach, however, gives an understanding of the basic anisotropies involved and establishes a framework for us to discuss these more complex reversal mechanisms. The energy equation takes the form:

$$E/M = -H \cos(\theta) - H_E \cos(\theta - \phi), \quad (1)$$

where H_E is the effective unidirectional anisotropy field, ϕ is the angle between the bias field H_b and the applied field H , and θ is the angle between H and the magnetization.¹ (This form ignores the induced uniaxial anisotropy in the NiFe layer, which is small compared to H_E .) Assuming the magnetization reorients by rotation following the minimum energy solution, the hard axis magnetization is:

$$\frac{M(H)}{M_s} = \frac{H}{\sqrt{(H^2 + H_E^2)}}. \quad (2)$$

Under these assumptions, the easy axis magnetization should have zero coercivity and change sign at $H = H_E$, and the hard axis magnetization should approach saturation asymptotically. The best fit of Eq. (2) to the measured hard axis magnetization for the polycrystalline film in Fig. 3(a) predicts $H_E = 83$ Oe which is inconsistent with the measured easy axis value of $H_E = 52$ Oe. By increasing the size of uniaxial anisotropy above the usual value for soft NiFe alloys, we can consistently model the easy and hard axis behavior observed in Figs. 3(a) and 4(a), and qualitatively account for the easy-axis coercivity:

$$E/M = -H \cos(\theta) - H_E \cos(\theta - \phi) + H_K \cos^2(\theta - \phi). \quad (3)$$

The predicted analytical form of $M(H)$ is complicated. However, the easy and hard axis behavior can now be modelled with $H_E = 53$ Oe and $H_K = 30$ Oe, given that Eq. (3) predicts that the hard-axis magnetization curve approaches saturation with $H_s \approx 2(H_E + H_K)$. The uniaxial term is significantly larger than that observed in films of NiFe without bias layers (H_K of NiFe = 5 Oe).³³ The increase of H_K is a manifestation of the interfacial interaction with the NiO. Uniaxial strain induced at the NiO/NiFe interface may be a source of uniaxial anisotropy, however, the small saturation magnetostriction expected for this composition of permalloy, combined with the small tetragonal distortion of the NiO below its Néel temperature make this an unlikely explanation for the large uniaxial anisotropy observed here.¹⁰

The large uniaxial term in the energy equation needed to consistently model the easy and hard axis data helps to account for the coercivity in the easy axis loop. It is well known that, in the presence of a uniaxial term, the energy equation contains local energy minima in addition to global minima for a range of applied fields.^{38,39} Local energy minima can pin the magnetization and temporarily delay the obtainment of the absolute energy minimum configuration. Assuming the NiFe moment in the biased bilayers reverses by rotation and follows the local energy minimum, the easy axis coercivity predicted by Eq. (3) is $H_{ce} = H_K = 30$ Oe. In unbiased NiFe films, however, $H_{ce} < H_K$ indicating the reversal occurs through domain wall motion rather than rota-

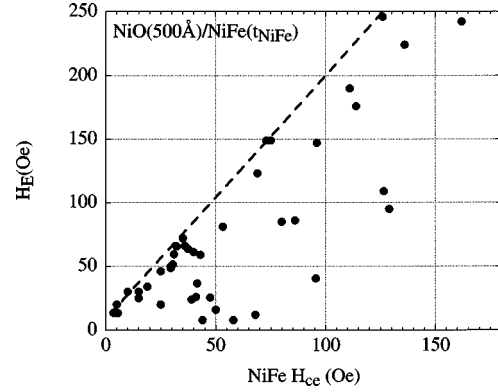


FIG. 6. The exchange anisotropy field, H_E for a wide variety of NiO-500 Å/NiFe- t_{NiFe} films plotted vs the easy-axis coercivity, H_{ce} . The dotted line is a guide to the eye indicating the relationship $H_E = 1.8H_{ce} + 14$ Oe, so the H_E to H_{ce} ratio has a limiting value of about 1.8. This value appears to be a characteristic of the AF material since the ratio observed for NiCoO/NiFe bilayers typically exceeds this value. AF/NiFe bilayers using Mn-based antiferromagnetic layers greatly exceed this value, giving much less coercivity per unit exchange anisotropy shift.

tion. The easy axis energy surfaces predicted by Eq. (1) for biased NiFe films do not contain local minima, unlike the energy surfaces described by Eq. (3) for biased films. Thus Eq. (3) containing uniaxial and unidirectional anisotropy terms is more consistent with the NiFe behavior.

It is interesting to note that the ratio of the H_E to H_{ce} for a wide range of IBS polycrystalline NiO/NiFe bilayers appears to have a characteristic maximum value. Figure 6 shows H_E plotted vs H_{ce} . The dotted line is a guide to the eye showing $H_E = 1.8H_{ce} + 14$ Oe. Figure 6 implies that increases in H_E and H_{ce} are correlated in the best polycrystalline NiO/NiFe bilayers and are thus different manifestations of the same surface anisotropy. On the other hand, films with small H_E and large H_{ce} occur since there are many sources of coercivity in thin NiFe films, many not directly related to the surface exchange interaction. H_E to H_{ce} ratios for NiO/NiFe bilayers published in the literature^{13,16} deposited using reactive sputtering are approximately 2.2, which are similar to the values observed in the IBS films. More recently, H_E to H_{ce} ratios of 9 have been reported in NiO/NiFe bilayers with carefully controlled interfacial roughness.⁴⁰

The slope of the line in Fig. 6 depends on the intrinsic anisotropies present in NiO. The H_E/H_{ce} ratios we observe in IBS-grown NiFe/NiCoO bilayers typically lie above this line. Further, a typical H_E/H_{ce} ratio for NiFe/FeMn bilayers is 25.⁶ The higher ratio observed in general in Mn-based AF exchange couples may be due to the higher magnetocrystalline anisotropy or the reduced symmetry of the Mn-based antiferromagnets.^{6,13} These differences produce an interface anisotropy that is more closely described by a pure unidirectional in FeMn/NiFe bilayers compared to the unidirectional plus uniaxial anisotropy found in NiO/NiFe bilayers.

Turning now to the magnetization observed in the epitaxial bilayers in Figs. 3(b) and 4(b), the shape of the hard-axis magnetization curves can be predicted by adding a cubic anisotropy to the energy equation (1):

$$H_{k1} \sin^2(\theta - \phi) \cos^2(\theta - \phi). \quad (4)$$

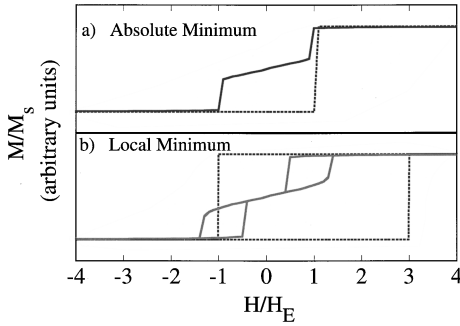


FIG. 7. Calculated easy axis (dashed) and hard axis (solid) magnetization loops using an energy equation with a unidirectional and cubic anisotropy [Eq. (5)]. In (a) we assume the magnetization achieves the absolute minimum energy configuration. In (b) we assume the magnetization remains in local minima until the path to the absolute minimum is unobstructed by an energy barrier. The calculations qualitatively reproduce the features observed in the epitaxial NiO/NiFe bilayers.

The data in Fig. 3(b) are reasonably well reproduced with $H_E = 20$ Oe, $H_{K1} = 30$ Oe. The cubic anisotropy produces an energy minimum perpendicular to the unidirectional anisotropy (and to H_b) which qualitatively changes the hard axis loop shape.

In addition, the presence of a cubic anisotropy produces local energy minima in the energy surface describing the bilayer magnetization reversal. As discussed previously, these minima can be used to qualitatively account for the coercivity observed in the hard axis magnetization loop. Qualitatively, as H decreases from a large positive value, the NiFe layer moment at first remains in a local energy minimum parallel to H , and then shifts suddenly from that minimum to the energy minimum derived from the unidirectional anisotropy term, perpendicular to H and parallel to H_b . Transverse magnetization data [Figs. 3(c) and 4(c)] for $H \perp H_b$ reinforce this description. As the longitudinal magnetization (M_x) decreases, the transverse magnetization (M_y) increases abruptly and reaches a plateau as the NiFe layer moment settles into the global energy minimum perpendicular to H . This is in contrast to the transverse hard-axis behavior of the polycrystalline bilayer couple which shows a smooth rotation of the NiFe layer moment and no plateau.

Calculated magnetization curves that qualitatively reproduce the experimental data for the epitaxial bilayers are shown in Figs. 7(a) and 7(b). The curves were calculated using an energy equation with a unidirectional and a cubic anisotropy:

$$E/(M^*H_E) = -H/H_E \cos(\theta) - \cos(\theta - \phi) + H_{K1}/H_E \cos^2(\theta - \phi) \sin^2(\theta - \phi) \quad (5)$$

where $H_{K1}/H_E = 1.5$. The magnetization in Fig. 7(a) is assumed to reverse by rotation and to find the absolute minimum energy configuration. The calculation reproduces the steps observed in the epitaxial hard axis loops. As in the case of the polycrystalline bilayers, if we assume the vector magnetization sticks in local energy minima and only achieves the absolute minimum when its path is unobstructed by an

energy barrier, we can qualitatively account for the coercivity observed in the easy and hard axis loops as shown in Fig. 7(b).

From the similarity of the hard axis loops in Figs. 3(b),3(c) and 4(b),4(c), where the bias field is applied along a different NiO crystal axis, it is clear that the cubic term is induced by the bias field applied during deposition, and is not referenced to the NiO or the NiFe crystal axes. Thus the data are not consistent with a magneto-crystalline anisotropy in the NiFe or the NiO. In contrast, epitaxial NiFe films deposited directly on MgO (001) show induced bulk uniaxial and cubic magnetocrystalline anisotropy terms which are nearly an order of magnitude smaller than those needed to describe the NiO/NiFe loops. The cubic anisotropy must arise from the same interfacial interaction with the NiO that produces the exchange anisotropy. We speculate that the reduced disorder at the epitaxial NiO surface relative to the polycrystalline NiO surface allows a more coherent response of the NiO spin configuration to the alignment of the NiFe grown on top of it. Ferromagnetic resonance or Brillouin light-scattering measurements on these bilayer films may give a more quantitative determination of the anisotropy values.

Our analysis treats the NiFe as an isolated layer under the influence of a static surface anisotropy produced by the NiO interface. This analysis implies that the spin configuration in the NiO layer undergoes reversible dynamics only during the reversal of the NiFe moment, which is incorrect strictly speaking. The observation of a training effect and the presence of rotational hysteresis in NiFe/NiO bilayers even at very high applied fields⁴¹ clearly show that some irreversible NiO wall motions occur during a NiFe reversal. However, a static induced surface anisotropy does describe many of the main features of the NiFe/NiO magnetization curves. The contributions of irreversible NiO spin dynamics on the NiFe loop are secondary effects in these experiments. Additional experimental work is needed to measure and understand the NiO wall motion during the NiFe magnetization reversal process.

Once again it is interesting to compare the behavior of NiFe/NiO and NiFe/FeMn exchange couples. As with NiO/NiFe exchange couples, there is a strong deposition order dependence in NiFe/FeMn exchange couples. However, in the FeMn case it is the NiFe that should be deposited first in order to achieve a large exchange bias.⁴⁵ The order dependence of NiFe/FeMn exchange bias has been found to arise from changes in growth mode when the order of deposition is reversed. The (111) textured NiFe surface serves as a template for the antiferromagnetic γ phase of FeMn. In the absence of the NiFe template the FeMn does not achieve the γ phase and instead forms in the nonmagnetic α phase, and no exchange bias is observed. In experiments where the γ FeMn is stabilized through epitaxy with a single crystal substrate, exchange bias is observed in NiFe deposited on top.⁶ Further, when the γ FeMn was grown in different crystalline orientations, exchange bias in the NiFe grown on top was observed in every case.⁶ The ratio of H_E to H_{ce} for the FeMn/NiFe bilayers was different for the different crystalline orientations, however.⁶ Features in the magnetization loops associated with uniaxial or cubic anisotropies in addition to the unidirectional anisotropy in epitaxial FeMn/NiFe bilayers

were not reported. Changing the order of NiO/NiFe bilayer deposition does not change the crystalline phases of the individual layers, but instead produces changes in growth mode that lead to differences in the exchange anisotropy.

We would like to discuss one final experimental fact we observed in NiO/NiFe bilayers, and that is the large exchange bias observed in as-deposited bilayers. Exchange bias in as-deposited films is also observed in NiFe/FeMn bilayers. Since bilayers are nominally deposited at room temperature, one might predict that as-deposited films would not exhibit exchange bias until they were heated above T_b and cooled in a field. The presence of exchange bias in as-deposited films implies that the temperature of the growing film exceeds T_b during the deposition. In order to test this hypothesis, we deposited NiO/NiFe bilayers on substrates clamped to a thick Cu plate that was cooled to -120°C . Large loop shifts H_E were still observed in these films. It is likely that even when the substrates are cooled from the back side, the energy transported to the film surface by the deposited material raises the surface temperature of the growing film above T_b . A more effective test of the above hypothesis would be to employ a low energy NiFe deposition technique such as evaporation in conjunction with substrate cooling. In an all metal system such as NiFe/FeMn, where the thermal conductivity is higher, maintaining a film temperature below T_b during deposition may be more straightforward.

Our observations on epitaxial oxide-AF/NiFe exchange-coupled bilayers are consistent with the unpublished data of Carey *et al.* who did extensive characterization of exchange couples using epitaxial NiO, NiCoO films and NiO/CoO multilayers grown by reactive magnetron sputtering.⁴² They report consistently smaller H_E in epitaxial relative to polycrystalline bilayers deposited under similar conditions. They also observe exchange anisotropy in both (111) and (001) oriented epitaxial bilayers, with consistently larger coercivity in the (111) relative to the (001) oriented films. Lai *et al.*⁴³ report loop shifts in bilayers with epitaxial (001) and (111) NiO films grown by metal-organic chemical vapor deposition (MOCVD). They observe unusually large and nearly isotropic coercivity in both (001) and (111) oriented MOCVD based bilayer couples, however. van der Zaag *et al.* have experimentally demonstrated the occurrence of exchange biasing in compensated epitaxial (100) Fe₃O₄/CoO multilayers.⁹

V. DISCUSSION

By definition, exchange bias is an uncompensated interaction between the antiferromagnetic and ferromagnetic layers. It has been well established that the loop shift is strictly an interfacial phenomena with regard to the NiFe (ferromagnetic) layer. The critical thickness in the NiO layer below which loop shifts are not observed indicates the presence of an intermediate region in the AF layer where the bias direction is stored in the spin configuration. Our data show that the interfacial spin configuration in the AF layer is not strongly influenced by the crystallographic orientation of the NiO layer. Instead, the indirect influence of the applied field through alignment of the NiFe layer and the strong NiO/NiFe interfacial interaction together determine the spin arrangement in the antiferromagnet interfacial layer and therefore

the bias direction. Disorder in the form of a polycrystalline film appears to enhance the loop shift due to stronger pinning of the AF spin configuration. Weaker pinning of the spins in the epitaxial NiO layer gives a reduced loop shift and a more complex induced surface anisotropy. Thus, the crystalline texture and degree of disorder at the interface control the NiO spin dynamics during the NiFe reversal. We do not observe irreversible NiO spin dynamics during the NiFe reversal (i.e., there is no training effect). On the contrary, the NiFe reversal is reasonably well described by a rotational model in a static effective surface anisotropy. The complex surface anisotropy is consistent with reversible rotational spin dynamics in the AF layer during NiFe reversal.

The model proposed by Mauri indicates that for sufficiently strong coupling at the FM/AF interface, FM reversal occurs through the formation of a domain wall in the AF layer parallel to the interface. The 180° wall does not annihilate and stores the bias direction information. Although Mauri assumes the AF interface is completely uncompensated, his conclusions for strong coupling hold independent of the detailed relationship between the AF and FM spins at the interface. Koon recently showed that the spins at a compensated AF interface may through a spin-flop mechanism rotate perpendicular to the FM alignment direction.⁴⁴ Koon's micromagnetic calculations for strong coupling of this type confirmed Mauri's analytical solutions and showed that the bias direction information can be stored in an 180° domain wall parallel to the interface. These models predict a critical thickness ($t = \pi \sqrt{A_{AF}/K_{AF}}$) for the AF layer that is greater than or equal to the AF domain wall thickness. Experimental critical thicknesses, however, are typically an order of magnitude smaller than predicted.

In general, interfacial roughness, stress and domains in the AF layer are likely to result in competing interactions on the AF spins at the interface which would produce a disordered interfacial spin configuration. Such a picture is consistent with the one presented by Stoecklein *et al.*⁴⁵ and Schlenker *et al.*⁴⁶ who suggest that the frustrated interactions at the AF/F interface may be similar to those in a spin glass. The blocking temperature for AF/F coupled layers is then analogous to the glass transition temperature in a system such as CuMn at which temperature the spins freeze into one of many disordered configurations. At the AF/FM interface, each disordered configuration may produce slightly different values of H_E . Dynamics in a spin glass occur over a very broad distribution of time scales, resulting in stretched exponential relaxation of H_E with time.⁴⁷ Once the interfacial spins are locked together, bias direction information can be stored in a disordered analog to the 180° domain wall proposed by Mauri. Experimental determination of the temperature dependence of the AF critical thickness (equivalent to the AF thickness dependence of the blocking temperature) in epitaxial NiO bias exchange couples may distinguish between these two models through comparison with the temperature dependence of the AF domain wall thickness.

VI. CONCLUSIONS

We have shown that polycrystalline NiO/NiFe bilayers produce larger loop shifts than epitaxial bilayers deposited simultaneously. The data indicate that a larger surface anisot-

ropy is induced at a polycrystalline relative to an epitaxial interface. The presence of exchange anisotropy in (001)-oriented epitaxial NiO/NiFe layers shows that the interfacial spin arrangement predicted by the bulk spin structure does not determine whether exchange bias is observed. In addition to the induced surface unidirectional anisotropy, an induced cubic surface anisotropy is needed to consistently model the hysteresis loops measured in epitaxial NiO/NiFe bilayers. Hysteresis loops of polycrystalline bilayers are most accurately modeled by an induced surface unidirectional anisotropy plus an enhanced uniaxial anisotropy. The induced surface anisotropies we observe are referenced only to the bias field applied during deposition, and are independent of the NiO crystalline orientation.

ACKNOWLEDGMENTS

Part of this work was performed under the auspices of the U.S. Department of Energy (DOE) by LLNL under Contract No. W-7405-ENG-48, and part was supported by DOE's Tailored Microstructures in Hard Magnets Initiative. L.E.J. was supported by DOE's Science and Engineering Research Semester, and Partners in Industry and Education programs. We would like to thank Matt Carey and Chih-Huang Lai for helpful discussions. We thank Y. K. Kim and Quantum Peripherals Colorado, Inc. for their support during the early stages of this project. We thank Ron Musket for RBS measurements and Norm Koon for making his results available to us prior to their publication.

*Now at Seagate Technology, 7801 Computer Avenue South, Minneapolis, MN 55435. Electronic address: Richard_P_Michel@notes.seagate.com.

†Now at Thin Film Department, Mailstop 2U-20, Hewlett Packard, 1501 Page Mill Road, Palo Alto, CA 94304. Electronic address: chaiken@hpl.hp.com.

- ¹W. H. Meiklejohn and C. P. Bean, *Phys. Rev.* **105**, 904 (1956).
- ²A. Yelon, in *Physics of Thin Films*, edited by H. Francombe and R. W. Hoffman (Academic Press, New York, 1971).
- ³A. P. Malozemoff *J. Appl. Phys.* **63**, 3874 (1988).
- ⁴D. Mauri, H. C. Siegmann, P. S. Bagus, and E. Kay, *J. Appl. Phys.* **62**, 3047 (1987).
- ⁵S. Soeya, T. Imagawa, K. Mitsuoka, and S. Narishige, *J. Appl. Phys.* **76**, 5356 (1994).
- ⁶R. Jungblut, R. Coehoorn, M. T. Johnson, J. aan de Stegge, and A. Reinders, *J. Appl. Phys.* **75**, 6659 (1994).
- ⁷A. J. Devasahayam and M. H. Kryder, *IEEE Trans. Magn.* **31**, 3820 (1995).
- ⁸J. X. Shen and M. T. Kief, *J. Appl. Phys.* **79**, 5008 (1996).
- ⁹P. J. van der Zaag, A. R. Ball, L. F. Feiner, R. M. Wolf, and P. A. A. van der Heiden, *J. Appl. Phys.* **79**, 5103 (1996).
- ¹⁰D. H. Han, J. G. Zhu, J. H. Judy, and J. M. Sivertsen, *J. Appl. Phys.* **81**, 340 (1997).
- ¹¹T. J. Moran, J. M. Gallego, and I. K. Schuller, *J. Appl. Phys.* **78**, 1887 (1995).
- ¹²H. Kanai, K. Yamada, K. Aoshima, and Y. Ohtsuka, *IEEE Trans. Magn.* **32**, 3368 (1996).
- ¹³T. Lin, C. Tsang, R. E. Fontana, and J. K. Howard, *IEEE Trans. Magn.* **31**, 2585 (1995).
- ¹⁴Y. Hamakawa, H. Hoshiya, T. Kawabe, Y. Suzuki, R. Arai, K. Nakamoto, M. Fuyama, and Y. Sugita, *IEEE Trans. Magn.* **32**, 149 (1996).
- ¹⁵P. Ciureanu, in *Thin Film Resistive Sensors*, edited by P. Ciureanu and S. Middelhoek (Institute of Physics, Philadelphia, PA, 1992).
- ¹⁶C.-L. Lin, J. M. Sivertsen, and J. H. Judy, *IEEE Trans. Magn.* **31**, 4091 (1995).
- ¹⁷M. J. Carey and A. E. Berkowitz, *Appl. Phys. Lett.* **60**, 3060 (1992).
- ¹⁸T. J. Moran, Ph.D. thesis, University of California at San Diego, 1995.
- ¹⁹J. Noguees, D. Lederman, T. J. Moran, and I. K. Schuller, *Phys. Rev. Lett.* **76**, 4624 (1996).

²⁰M. M. Farztdinov, *Usp. Fiz. Nauk* **84**, 855 (1964).

²¹W. L. Roth, *Phys. Rev.* **110**, 1333 (1958).

²²W. L. Roth, *Phys. Rev.* **111**, 772 (1958).

²³A. J. Sievers and M. Tinkham, *Phys. Rev.* **129**, 1566 (1962).

²⁴G. A. Slack, *J. Appl. Phys.* **31**, 1571 (1960).

²⁵T. R. McGuire and W. A. Crapo, *J. Appl. Phys.* **33**, 1291 (1962).

²⁶W. L. Roth and G. A. Slack, *J. Appl. Phys.* **31**, 1571 (1960).

²⁷S. Saito, M. Miura, and K. Kurosawa, *J. Phys. C* **13**, 1513 (1980).

²⁸A. Chaiken, R. P. Michel, and C. T. Wang, *J. Appl. Phys.* **79**, 4772 (1996).

²⁹A. Chaiken, R. P. Michel, and M. A. Wall, *Phys. Rev. B* **53**, 5518 (1996).

³⁰R. P. Michel, A. Chaiken, Y. K. Kim, and L. E. Johnson, *IEEE Trans. Magn.* **32**, 4651 (1996).

³¹Cerac Inc., Milwaukee, WI 53201-1178.

³²J. M. Florczak and E. D. Dahlberg, *Phys. Rev. B* **44**, 9338 (1991).

³³S. Chikazumi, *Physics of Magnetism* (Wiley, New York, 1964).

³⁴T. Ambrose and C. L. Chien, *Appl. Phys. Lett.* **65**, 1967 (1994).

³⁵B. A. Everitt, D. Wang, and J. M. Daughton, *IEEE Trans. Magn.* **32**, 4657 (1996).

³⁶V. I. Nikitenko, V. S. Gornakov, L. M. Dedukh, Yu. P. Kabanov, A. F. Khapikov, A. J. Shapiro, R. D. Shull, A. Chaiken, and R. P. Michel, *J. Appl. Phys.* **83**, 6828 (1998).

³⁷M. T. Kief, *J. Appl. Phys.* **81**, 4981 (1997).

³⁸B. Dieny, J. P. Gavigan, and J. P. Rebouillat, *J. Phys.: Condens. Matter* **2**, 159 (1990).

³⁹B. Dieny and J. P. Gavigan, *J. Phys.: Condens. Matter* **2**, 187 (1990).

⁴⁰D. H. Han, J. G. Zhu, J. H. Judy, and J. M. Sivertsen, *Appl. Phys. Lett.* **70**, 664 (1997).

⁴¹D. Paccard, C. Schlenker, O. Massenet, R. Montmory, and A. Yelon, *Phys. Status Solidi* **16**, 301 (1966).

⁴²M. J. Carey, A. E. Berkowitz, J. A. Borchers, and R. W. Erwin, *Phys. Rev. B* **47**, 9952 (1993).

⁴³C.-H. Lai, H. Matsuyama, R. L. White, and T. C. Anthony, *IEEE Trans. Magn.* **31**, 2609 (1995).

⁴⁴N. C. Koon, *Phys. Rev. Lett.* **78**, 4865 (1997).

⁴⁵W. Stoecklein, S. S. P. Parkin, and J. C. Scott, *Phys. Rev. B* **38**, 6847 (1988).

⁴⁶C. Schlenker, S. S. P. Parkin, J. C. Scott, and K. Howard, *J. Magn. Mater.* **54-57**, 801 (1986).

⁴⁷M. B. Weissman, *Rev. Mod. Phys.* **65**, 829 (1993).